Article

Numerical Study on Self-Propulsion Performance of Underwater Vehicle Based on CFD

Jiyuan Sun[1], Chenyu Pu[1,2], Bowen Zhao[3]

[1] Ocean College, Zhejiang University, 316000, Zhejiang Zhoushan, China;
[2] State Key Laboratory of Satellite Ocean Environment Dynamics, Second Institute of Oceanography, Ministry of Natural Resources, 310012, Zhejiang, Hangzhou, China；
[3] Department of Applied Mathematics and Mathematical Modeling, Saint-Petersburg State Marine Technical University, Saint-Petersburg 190121, Russia

Abstract: This paper is based on the CFD method to numerically study the manoeuvrability of an underwater vehicle. By predicting the straight-line navigation resistance of the underwater vehicle, the results agreed well with the test values, which verified the accuracy of the numerical method. In addition, two methods of static and dynamic prediction were used to solve the self-propulsion point based on the body force method for the SUBOFF underwater vehicle with E1619 propeller, and ultimately the relative errors of the two methods of the propeller rotational speed and thrust were -1.56% and -4.54%, respectively. The performance parameters of the propeller thrust coefficient K_T and torque coefficient K_Q were also close to each other base on the two methods, and the relative errors were all within 3%. This paper provides a good foundation for the prediction of zigzag test, turning circle and other motions of the subsequent underwater vehicle, which is of great significance.

Keywords: underwater vehicle; self-propulsion; CFD; body force method

1. Introduction

Since the beginning of the 21st century, underwater vehicles have gradually become an important strategic research target. The maneuverability of underwater vehicle is one of the

Eng. Solut. Mech. Mar. Struct. Infrastruct., 2024, Vol. *1*, Issue 1

2 of 20

important performances to ensure its navigation safety, and the self-propulsion test is an important technical method to evaluate the maneuverability of ships and underwater vehicles. Due to the huge cost of the real ship test and the long test period, so finding a technical method with the advantages of economy and preparation accuracy is the key focus of the current maneuverability research field.

In recent years, hydrodynamic academics have carried out a large number of experimental and numerical computational studies on the maneuvering performance of underwater vehicles. At the same time, The computational fluid dynamics (CFD) has improved greatly in terms of computational capability and accuracy, providing effective solutions for solving the hydrodynamic performance of hulls and their surrounding complex flow fields, and there is a significant impact on the engineering practice.

At present, the application of CFD technology can not only simulate the underwater vehicles' constrained mode test, but also calculate and solve the maneuvering motion with multiple degrees of freedom. And the direct simulation of the underwater vehicle's maneuvering motion based on CFD technology has gradually become a research hotspot in this field. Yang et al. [1] investigated the hydrodynamic characteristics of a fully attached SUBOFF underwater vehicle with an E1619 propeller and obtained reliable self-propulsion data. Chase et al. [2] calculated the self-propelled parameters of the SUBOFF underwater vehicle with an E1619 propeller and analyzed the performance of the propeller, which provided important data references and supported for researches in this field. Li Peng et al. [3] used STAR-CCM+ software to numerical simulate the underwater vehicle's self-propelled model (SUBOFF with E1619 propeller) near the free surface. They found that the presence of the free surface mainly affected the pressure distribution on the propeller blade surface behind the underwater vehicle, and increased the propeller rotational speed corresponding to the self-propulsion point. Cosgun et al. [4] calculated the flow field around the SUBOFF underwater vehicle and found that the propeller rotational speed increased as the speed increased, while the advanced coefficient remained constant. Wang [5] completed a direct numerical simulation of the ship's course-keeping, zigzag test steering and turning circle motions based on overlapping mesh technology and motion feedback mechanism. Liao et al. [6] simulated the six-degree-of-freedom motion of an underwater vehicle's emergency ascent at a certain depth based on the VOF method and overlapping mesh technique. Zhou et al. [7] found that during underwater vehicle ascending, the change in longitudinal inclination angle was large, and instability of the roll is prone to occur when the underwater vehicle emerged from the water surface. Amiri et al. [8] conducted the static drift test on the SUBOFF model using the URANS method and Reynolds Stress Turbulence model, and observed a significant interaction between the low-pressure region generated by the leeward vortex structure and the free surface. Savas Sezen et al. [9] used steady-state RANS method and the *SST k-ω* turbulence model to solve the flow around three different scales of underwater vehicles with their propellers. It was found that the influence of scale effect on self-propulsion characteristics would decrease as the model length increased. Liu et al. [10] conducted self-propulsion simulation on the full-size SUBOFF underwater vehicle

and compared the simulation results with the model with added surface friction correction (size reduction by ten times). The wake fraction of the full-size model was lower than that of the model size, because the boundary layer on the full-size hull was thinner. They also found that the thrust coefficient K_T and torque coefficient K_Q will increase as the propeller size increased. Howan Kim et al. [11] developed a full six-degree-of-freedom CFD maneuvering model and performed straight-line and steady turning maneuvering motions on a JoubertBB2 underwater vehicle, and maneuvering characteristics obtained were in good agreement with the test data. P.M. Carrica et al. [12,13] studied the self-propelled motion of the JoubertBB2 underwater vehicle near the free surface using discrete propeller and overlapping mesh methods, and found that near-surface navigation generated considerable vertical forces and pitching moments, with the average thrust and torque coefficients in waves being slightly lower than those in calm water. And later it was found that the model dimensions would have a large effect on the forces exerted on the hull in the study of the underwater vehicle's -10°/10° zigzag motion, and that the propeller operating point would change significantly.

The most critical issue in direct CFD simulation is the coupling problem of the propeller. The current numerical methods for studying the underwater vehicle-propeller or ship-propeller coupling problem can be divided into two categories: the overall modelling method and the body force method. When the overall modelling method is used, the computational accuracy is high and the interaction between underwater vehicle and propeller can be reflected more accurately, but the computational efficiency is low; whereas the body force method is simple in modelling, high in computational efficiency, and can comprehensively predict flow field information. Zhan et al. [14] used overlapping mesh to process the multi-body motions of the S175 ship, and simulated the rotation of the propeller based on the body force method. The predicted rotational motion parameters of the propeller were in good agreement with the test data. Wang et al. [15] used the overall modelling method, descriptive body force method, and RANS-BEM iterative body force method to predict the propulsion performance of the KCS ship model. The results showed that the body force method can accurately predict the overall propulsion performance of the ship, and the RANS-BEM iterative body force method has higher computational efficiency compared to the traditional iterative body force method. Tan et al. [16] found that there was not much difference in the calculation results between the overall modelling method and the body force method when studying the overall maneuverability of KVLCC2 ship-propeller-rudder. Wang et al. [17] simulated the oblique motion, the yaw motion, the combination of yaw and drift angle motion on Planar Motion Mechanism (PMM), and the athwartship force *Y*, the yawing moment *N*, and the heeling moment *K* are also acquired. The simulation results are then compared with the actual test results, which demonstrated the feasibility of the proposed method in PMM simulation. Wei et al. [18] carried out the numerical simulation of underwater vehicle emergency surfacing motion at different speeds based on a simplified model of propeller volume force. As the results show, the faster the rotation speed, the shorter the time for the underwater vehicle to gain steady speed and maintain fixed depth underwater. At the same time, with the increase in rotation speed, the fluctuation time of trim angle increases, while

the fluctuation time of heeling angle decreases. Wu et al. [19] used the body force method to numerical simulate the self-propulsion performance and steady turning motion of the ships, and found that the body force method has high accuracy in studying self-propelled motion.

Overall, the body force method is widely used in solving the self-propulsion performance of surface ships and underwater vehicles, which simplifies the modeling of propellers, improves computational efficiency, and can be used to simulate the turning, ascent, and other movements of ships and underwater vehicles during maneuvering. It is of great significance for simplifying their calculations of maneuverability. At present, the body force method is a precise and fast numerical method for predicting the self-propulsion performance of underwater vehicles, and it effectively solves the self-propulsion calculation in the absence of a three-dimensional model of the propeller. Therefore, this paper calculated the self-propulsion point of the SUBOFF underwater vehicle in deep water based on CFD and body force methods, and provided self-propulsion performance parameters for static and dynamic prediction. This provides reference significance for applying the body force method to solve the self-propulsion performance of other underwater vehicles.

2. Methodology

2.1 Governing equations

The three conservation equations of fluid flow are mass conservation equation, momentum conservation equation and energy conservation equation. Fluid is compressible, but in the hydrodynamic research of ships or submersibles, the water can be regarded as an incompressible fluid, which is true in general, and the velocity field and pressure field can be derived by the following formulas [20,21]:

$$\frac{\partial u_i}{\partial x_i} = 0 \tag{1}$$

$$\frac{\partial u_i}{\partial t} + \frac{\partial (u_i u_j)}{\partial x_j} = -\frac{1}{\rho}\frac{\partial p}{\partial x_i} + \frac{\partial}{\partial x_j}\left[\mu\left(\frac{\partial u_i}{\partial x_j} + \frac{\partial u_j}{\partial x_i}\right)\right] \tag{2}$$

In order to accurately simulate the turbulent motion, the variables in the equation need to be decomposed into two parts: time-averaged and pulsating:

$$\phi = \phi + \phi' \tag{3}$$

Then the time average of both sides of the equation can be obtained to calculate the RANS equation for incompressible fluids:

$$\frac{\partial u_i}{\partial x_i} = 0 \tag{4}$$

$$\frac{\partial u_i}{\partial t} + \frac{\partial (u_i u_j)}{\partial x_j} = -\frac{1}{\rho}\frac{\partial p}{\partial x_i} + \frac{\partial}{\partial x_j}\left[\mu\left(\frac{\partial u_i}{\partial x_j} + \frac{\partial u_j}{\partial x_i}\right)\right] \tag{5}$$

where u_i is the time-averaged velocity component $(u_1 = u, u_2 = v, u_3 = w)$ in the direction of the Cartesian coordinate system $x_i(i = 1,2,3)$, ρ is the mass density of fluid water, t is the time, p is the time-averaged pressure, μ is the molecular viscosity

coefficient, f_i is the component of the external force in the x_i direction, u_i' is the pulsating velocity component in the Cartesian coordinate $x_i(i = 1,2,3)$ direction, $\rho\overline{u_i'u_j'}$ is the Reynolds stress tensor.

2.2 Body force method

The body force method is to solve the RANS equations by substituting the volumetric force generated by the rotational motion of the propeller as a source term. According to the coupling form of the body force method and RANS equations can be divided into descriptive body force method and iterative body force method, the difference between these two is that the descriptive body force method only needs to calculate the wake flow field once, which can be substituting into the RANS equations for the subsequent solution, and the iterative body force method needs to be calculated in several iterations to update the information of the wake flow field continuously. In this paper, mainly adopting the descriptive body force method. The specific expression is as follows [22]:

$$f_{bx} = A_X r^* \sqrt{1 - r^*} \tag{6}$$

$$f_{b\theta} = A_\theta \frac{r^* \sqrt{1 - r^*}}{r^*(1 - r_h') + r_h'} \tag{7}$$

$$r^* = \frac{r - R_H}{R_P - R_H} \tag{8}$$

$$r_h' = \frac{R_H}{R_P} \tag{9}$$

where f_{bx} is the axial volume component force, $f_{b\theta}$ is the tangential volume component force, r is the radial coordinate position, R_P is the propeller radius, and R_H is the propeller hub radius, where A_x and A_θ are constants defined as follows:

$$A_x = \frac{105}{8} \cdot \frac{T}{\pi\Delta(3R_H + 4R_P)(R_P - R_H)} \tag{10}$$

$$A_\theta = \frac{105}{8} \cdot \frac{Q}{\pi\Delta R_P(3R_H + 4R_P)(R_P - R_H)} \tag{11}$$

where T is the thrust, Q is the torque and Δ is the thickness of the virtual disc body.

3. Computational model and meshing

3.1 Geometric models

This paper takes the full-attachment SUBOFF model as the object of study, which is proposed by the Defense Advanced Research Projects Agency (DARPA), including a

combination of attachments such as the axisymmetric body, the command console enclosure and the rudders. Figure. 1 is a schematic diagram of the fully attached SUBOFF, there is a pair of cross-shaped rudder and a command console enclosure located in the front end of the parallel midbody. The underwater vehicle views under different orientation are shown in Figure. 2. The specific parameters of the geometric model selected in this paper are shown in Table 1.
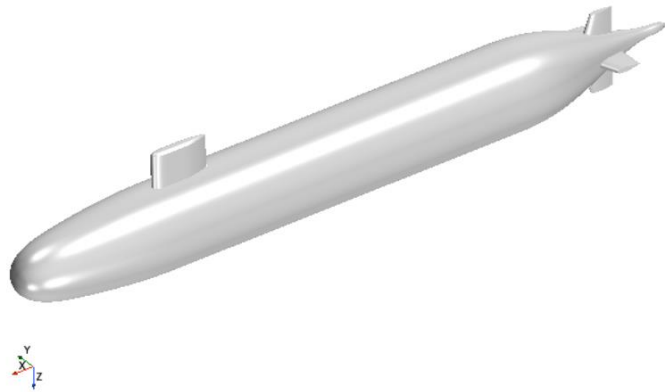

Figure. 1. Model diagram of fully attached SUBOFF underwater vehicle.

(A)

(B)

(C)　　　　　　　　　　　　　　　　(D)
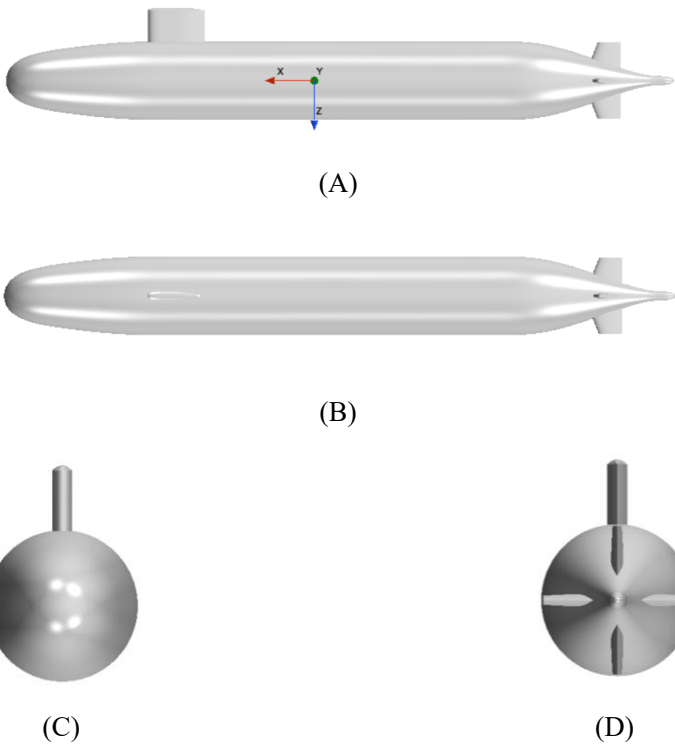
Figure. 2. Different views of fully attached SUBOFF underwater vehicle. (A) Positive along the y-axis. (B) Positive along the z-axis. (C) Reverse along x-axis. (D) Positive along the x-axis.

Table 1. Parameters of fully attached SUBOFF underwater vehicle.

Main characteristics	Units	Values

Overall Length L_{OA}	m	4.356
Length between perpendiculars L_{PP}	m	4.261
Maximum diameter D	m	0.508
Wetted surface S	m^2	6.348
Displacement ∇	m^3	0.706

3.2 Setup of calculation domain

The three-dimensional rectangular domain is selected for the calculation domain, its axis coincides with the symmetry axis of the underwater vehicle model, and the origin is located at the center of gravity of the underwater vehicle. It's extended forward for $2.5L_{OA}$ to the front boundary of domain and extended backward $3.0L_{OA}$ to the rear boundary of domain, with a distance of 8D from the surrounding sides.

The self-propulsion prediction method in this paper is divided into static prediction and dynamic prediction. The difference lies in whether the propeller directly drives the underwater vehicle forward. For the static prediction, the SUBOFF remains stationary and its self-propulsion point is found by determining the balance of thrust and drag by specifying the inflow velocity, and for the dynamic prediction, it is achieved by changing the propeller rotational speed to propel the underwater vehicle forward at the specified speed. The boundary condition settings for the computational domain are shown in Figure. 3.
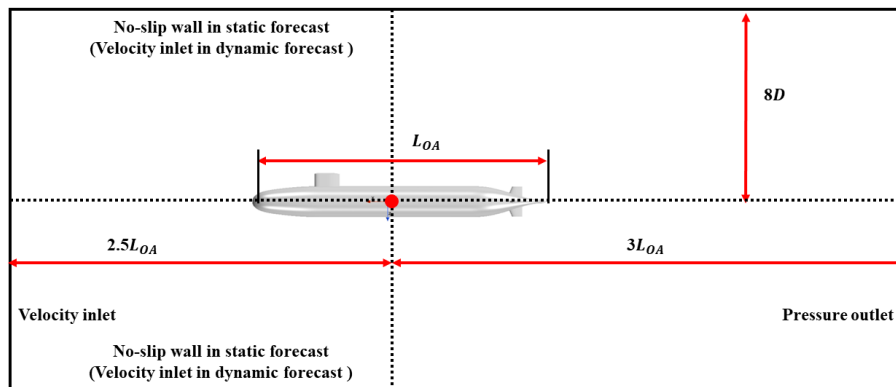

Figure. 3. Calculation domain and boundary conditions.

3.3 Mesh generation

The mesh generation is based on hexahedral mesh. In order to better capture the flow details, the multi-layer mesh encryption transition will be performed on the wake of the underwater vehicle and its surrounding domain, as shown in Figure. 4, and the surface mesh of the underwater vehicle is shown in Figure. 5.
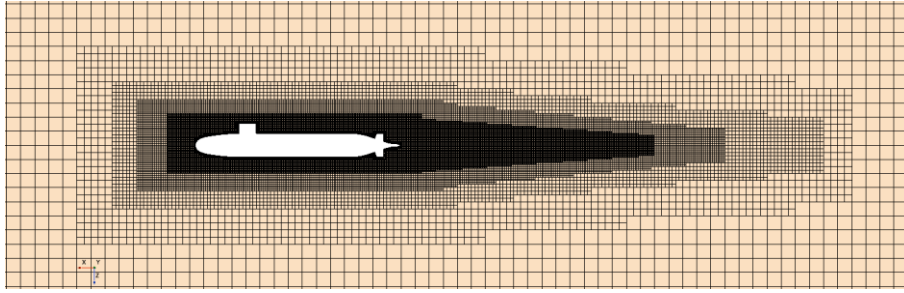
Figure. 4. Mesh division of computing domain.

Figure. 5. The surface mesh of the underwater vehicle.

The mesh type used for self-propulsion calculation in this paper is consistent with that used for the straight-line navigation resistance calculation. The difference lies in the mesh division at the propeller end of the underwater vehicle. Due to the use of body force method to simulate the propeller rotational motion, and there is no real propeller placed at the stern of the underwater vehicle, so there is no need to discretize the propeller blades and other components. However, it is necessary to refine the mesh in the virtual disk rotation domain of the propeller, to ensure accurate description of the surrounding rotating flow field information, the specific mesh division is shown in Figure. 6.
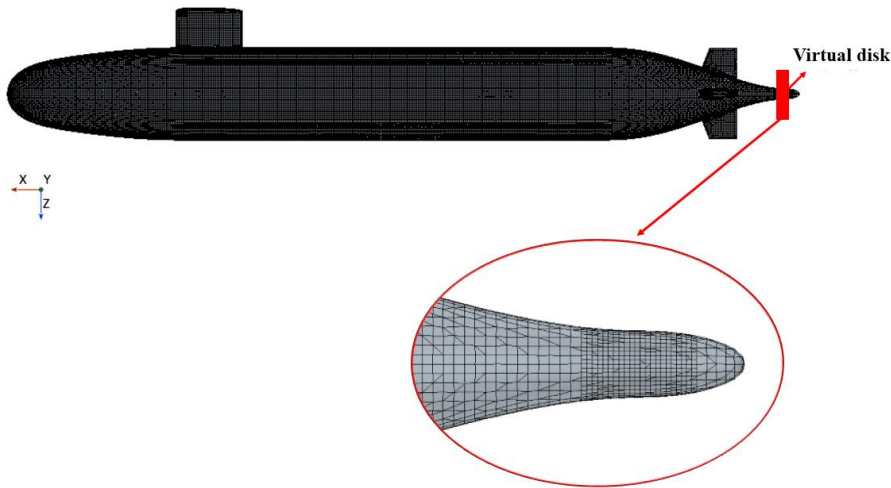

Figure. 6. Meshing of hull surface and virtual disk.

3.4 Verification and validation

3.4.1 Mesh convergence analysis

Before conducting the numerical simulation, it is necessary to verify the mesh-independence. In this paper, 8 sets of meshes are used to forecast the resistance of the

underwater vehicle with the speed of 10kn. And only the base size of the mesh is changed to get different number of mesh, in which the size of the prismatic layer and the encrypted domain remain unchanged. The results of the calculations are shown in Figure. 7.

Figure. 7 shows the comparison of the prediction of resistance values for SUBOFF underwater vehicle navigation at 10kn with different number of mesh, it can be concluded that with the increase of the number of mesh, the value of resistance decreases. When the number of mesh is greater than 2 million, the calculation results begin to converge. Taking into account the calculation efficiency and accuracy of the problem, the number of mesh used for the subsequent calculations is 2,393,000.
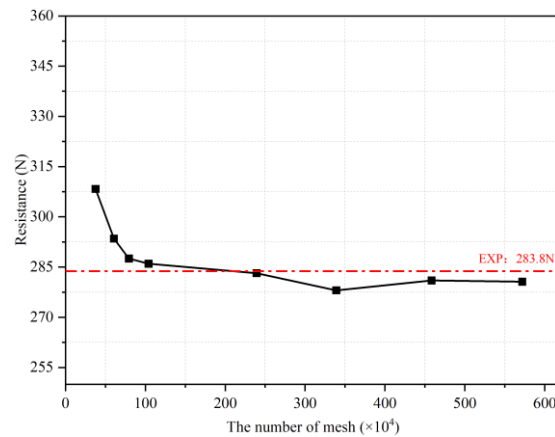

Figure. 7. Mesh convergence analysis.

3.4.2 Numerical verification

In this paper, the resistance calculation results of the SUBOFF underwater vehicle in straight- line navigation are compared with the experimental data measured by Roddy in the towing tank in 1990 [23,24], as shown in Table 2 and Figure. 8, which can be found that the simulated values of the resistance under different speeds are in good agreement with the experimental data. And with the increase of the underwater vehicle speed, the resistance increases continuously and the growth rate becomes faster. The relative errors between the resistance values predicted and the experimental data are within ±3%.

Table 2. Comparison of underwater vehicle resistance prediction under different speeds.

Velocity/kn	Test data/N	Simulation data/N	Relative error
5.93	102.3	104.27	1.93%
10	283.8	283.16	-0.22%
11.85	389.2	389.40	0.05%
13.92	526.6	527.06	0.09%
16	675.6	684.69	1.35%

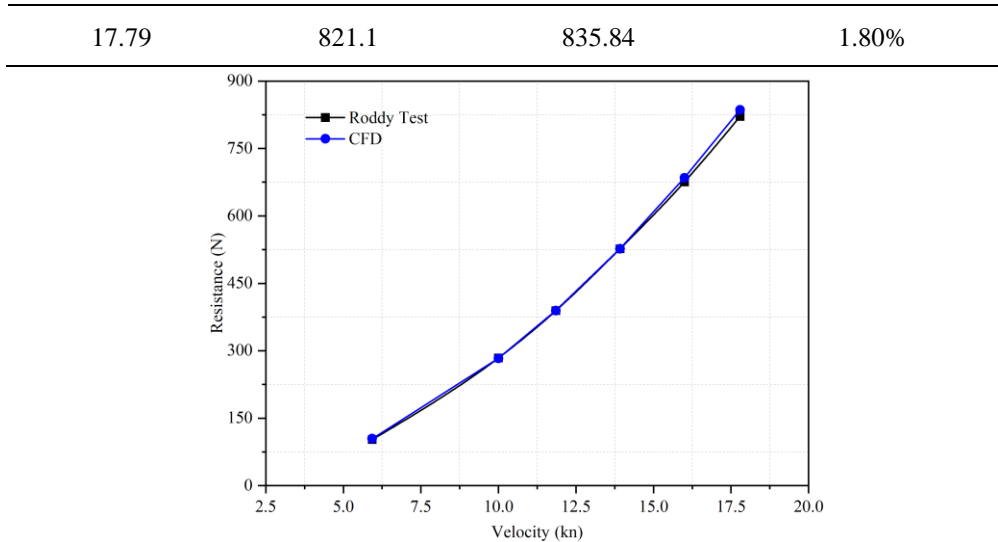| 17.79 | 821.1 | 835.84 | 1.80% |

Figure. 8. Predicted value of SUBOFF resistance at different speeds.

4. Results and Discussion

The research object of the self-propelled simulation is the combination of SUBOFF fully attached underwater vehicle with the E1619 propeller, in order to achieve interaction between the underwater vehicle, propeller, and rudders.

Before conducting the self-propulsion calculation of the SUBOFF underwater vehicle, it is necessary to determine the open water performance of the E1619 propeller, which means it needs to be subjected to open-water testing. The open-water test of E1619 propeller has been completed in CNR-INSEAN, Italy, and many scholars have also carried out CFD calculations on the open-water performance of E1619 propeller, and the results are in good agreement with the test values. The geometric model of E1619 propeller is shown in Figure. 9, and the open-water performance of E1619 propeller used in this paper is taken from the test data of Chase et al. [2], as shown in Figure. 10.
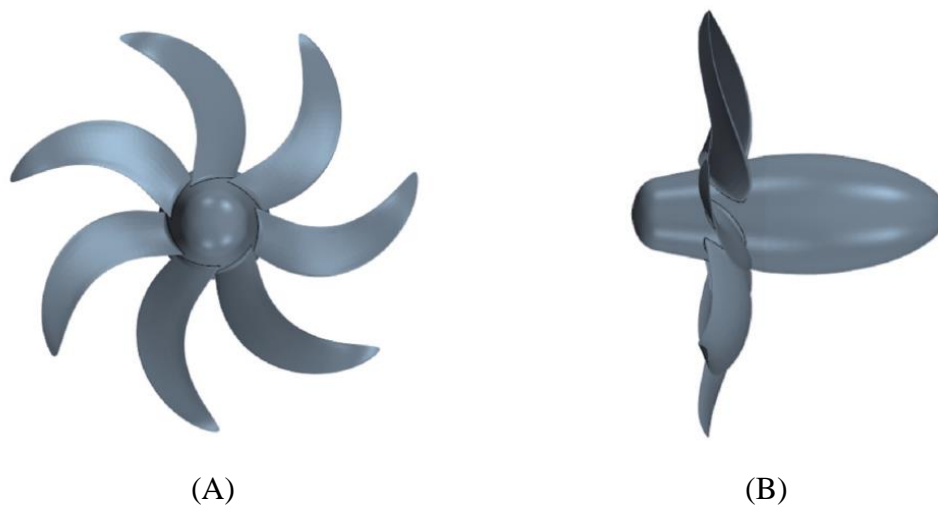

(A)   (B)

Figure. 9. Geometric model of E1619 propeller. (A) Front view. (B) Side view.
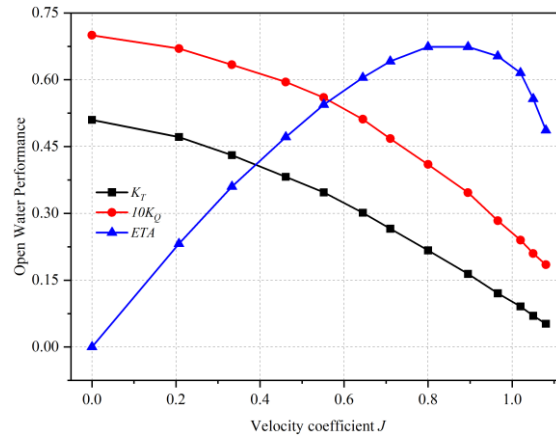
Figure. 10. Open water characteristic curve of the E1619 propeller.

4.1 Determination of self-propulsion point

4.1.1 The static forecast

This paper calculates the self-propulsion point when the underwater vehicle is navigating at the speed of 2.75m/s. The underwater vehicle resistance is 82.3 N at the given speed V_a is 2.75m/s, which is obtained by the interpolation of the straight-line navigation resistance curve in section 3.4.2. Based on the design reference value of underwater vehicles' thrust deduction coefficient (0.1~0.18) [1], the initial thrust deduction coefficient t_0=0.14 is assumed. And the thrust coefficient K_T corresponding to the maximum open-water efficiency is found on the given open-water characteristic curve of the E1619 propeller to obtain the initial propeller rotational speed n is 606 rpm.

During the static forecasting process, maintain the inlet velocity V=2.75m/s and Reynolds number Re=1.2×10^7. Figure. 11 shows the thrust and resistance values of the underwater vehicle under different propeller rotational speeds. As the propeller speed increases, the resistance of the underwater vehicle and the thrust of the propeller both show increasing trends, with the thrust increasing at a significantly higher speed than the resistance. Subsequently, the self-propulsion point is calculated using the cubic spline interpolation method, which are: the propeller rotational speed is 617.36rpm, at which the thrust and resistance are both equal to 96.45N.
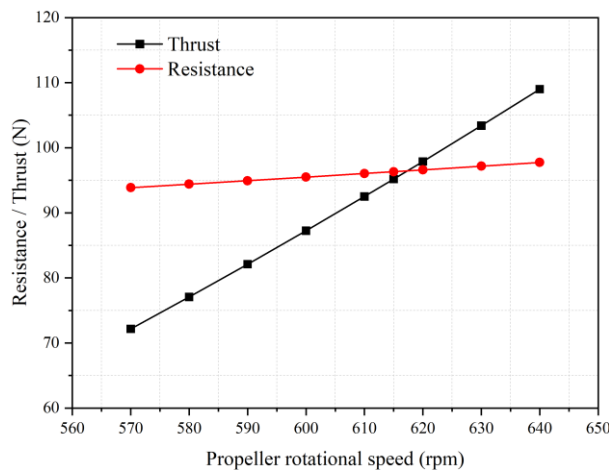

Figure. 11. Static forecasting results.

4.1.2 The dynamic forecast

The DFBI (Dynamic Fluid Body Interaction) model is used in the dynamic forecasting process, which can be used to calculate the forces and moments exerted by a rigid body in fluid and to simulate the relative motion between the fluid and the rigid body. By changing the rotational speed of the propeller several times, the speed of SUBOFF underwater vehicle at the time of convergence of thrust and drag is calculated until the speed reaches 2.75 m/s. The calculation results are shown in Figure. 12. The third spline interpolation method is used to obtain the propeller rotational speed of 607.7 rpm at the self-propulsion point, with the thrust and resistance equal to 92.068 N.
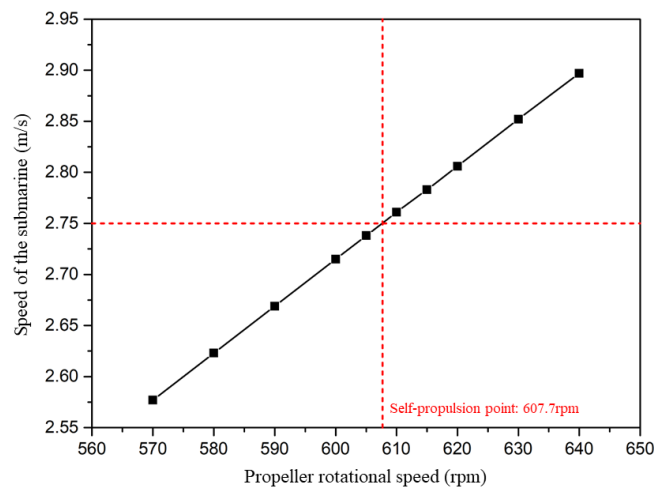

Figure. 12. Dynamic forecasting results.

The results of the comparison between static and dynamic forecasts are shown in Table 3, and the relative errors of thrust, drag and propeller rotational speed are all within 5%, which indicates that the calculation of the self-propulsion point by these two methods is relatively reliable. However, it is worth mentioning that in the process of static forecast, the results start to converge after 6.5s of calculation, whereas the results of the dynamic forecast need to be calculated for about 45s, which can be seen that in the case of similar results of the two methods, the choice of static forecast can greatly save the calculation time.

The self-propulsion point of the underwater vehicle derived from the dynamic forecast is substituted into the numerical model to calculate again, its speed and acceleration time history curves are shown in Figure. 13, with the acceleration decreasing to zero, the speed gradually converges to the stable value of 2.75 m/s. The time history curves of the thrust and resistance are shown in Figure. 14, the thrust and resistance eventually stabilized at 92.068N.

Table 3. Comparison of static prediction and dynamic prediction results.

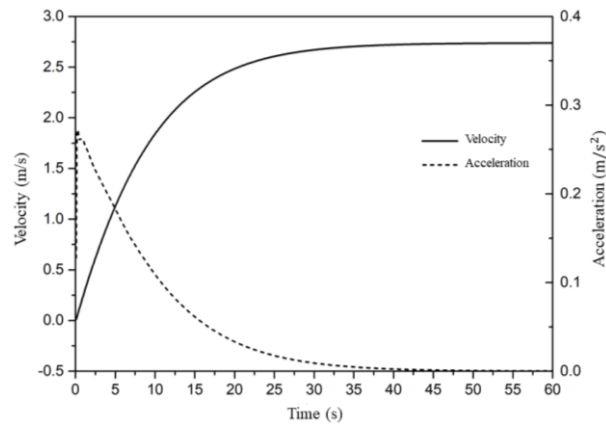| Methods	Thrust/N	Relative Error	Propeller rotational speed /rpm	Relative Error
The static forecast	96.450	-	617.360	-
The dynamic forecast	92.068	-4.54%	607.700	-1.56%

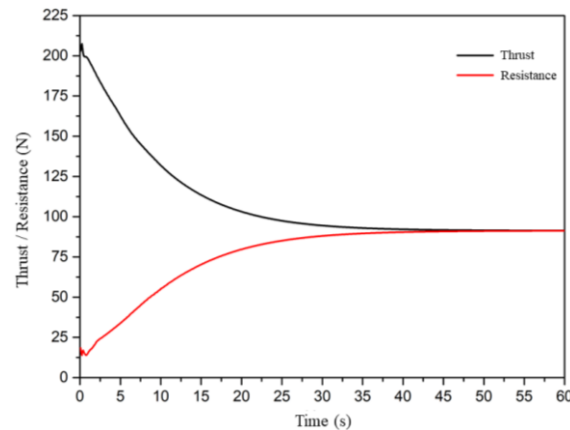**Figure. 13. Time history curves of the dynamic forecasting speed and acceleration.**


Figure. 14. Time history curves of the dynamic forecasting of thrust and resistance.

4.1.3 Flow field analysis

The velocity distribution of the underwater vehicle's mid longitudinal section obtained from static and dynamic forecasting calculations is shown in Figure. 15. During the dynamic forecasting process, the velocity field around the hull shows a flowing state. In the flow field domain of the propeller, it is evident that a strip shaped wake is generated due to the rotation of the propeller. The velocity nephogram of the propeller disc (x=0.978L) is shown in Figure. 16. The velocity field forecasted by both methods are similar, with a "four-leafed-clover" shape.
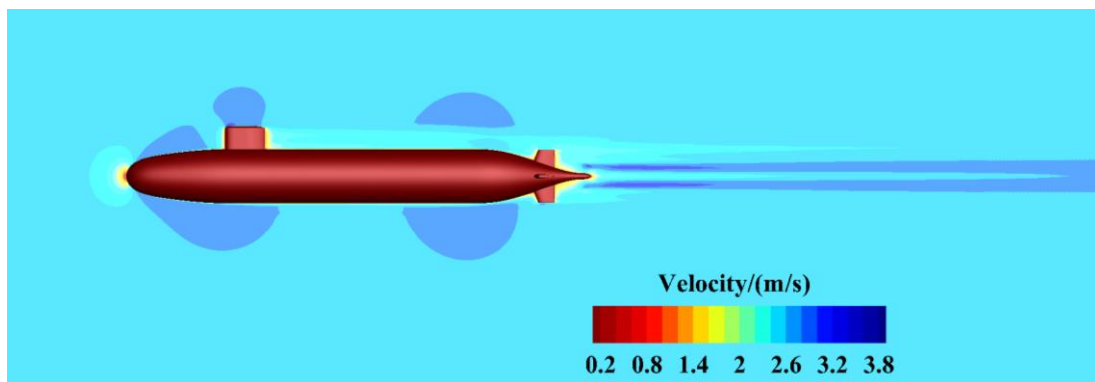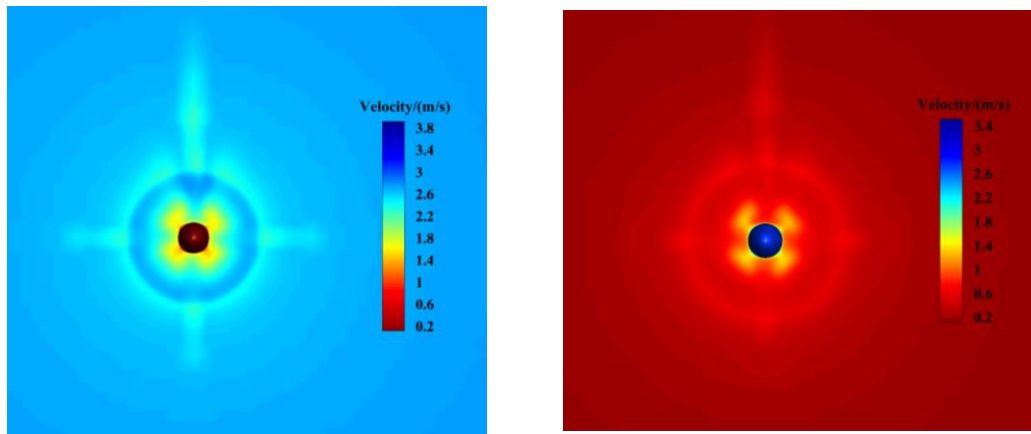

(A)
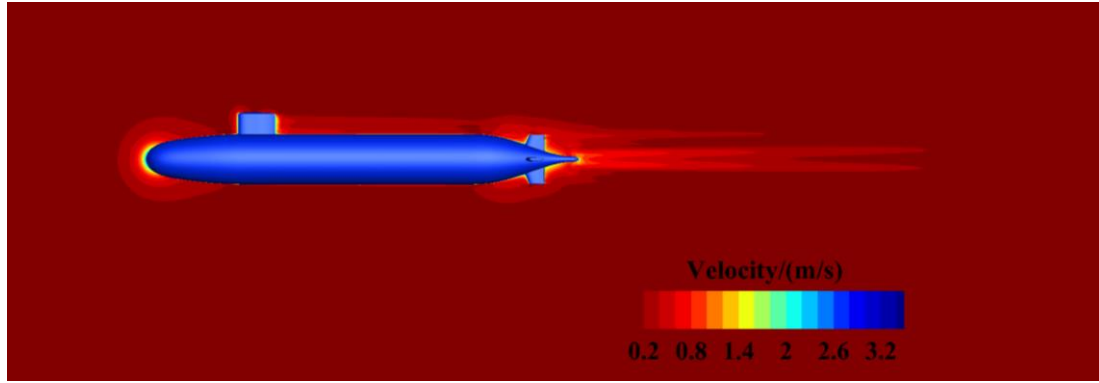
(B)

Figure. 15. Velocity nephogram of self-propelled predicted (middle longitudinal section). (A) Static forecast. (B) Dynamic forecast.

(A)   (B)

Figure. 16. Velocity nephogram of self-propelled predicted (propeller disk x = 0.978L).

(A) Static forecast. (B) Dynamic forecast.

The vortex structures under the self-propulsion point are shown in Figure. 17, which are described based on the Q criterion (Q=10). The vortex structures obtained by static and dynamic forecasting methods are basically the same, and the vortex structures in the propeller domain is reflected in a circular shape, which are different from that generated by the real propeller rotation. It cannot capture the tip vortex and blade root vortex well, but can capture the tail wing vortex and the horseshoe vortex at the enclosure.
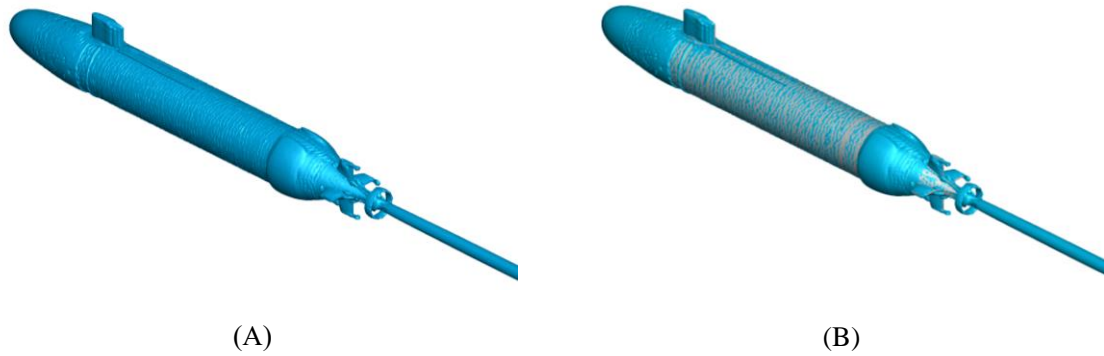
(A)   (B)

Figure. 17. Vortex structures of SUBOFF underwater vehicle self-propelled (Q = 10 iso-surface). (A) Static forecast. (B) Dynamic forecast.

4.2 Self-propulsion performance parameters

During the self-propelled process of the underwater vehicle, the interaction between the hull and the propeller is mainly manifested in the following three aspects, as shown in Figure. 18:

(1) The flow fluid behind the underwater vehicle has an impact on the inflow of the propeller, resulting in the inflow velocity V_A of the propeller is less than the actual underwater vehicle speed V_S;

(2) The rotation of the propeller behind the hull affects the flow field around the hull, resulting in the actual required thrust T being greater than the resistance R of the bare hull;

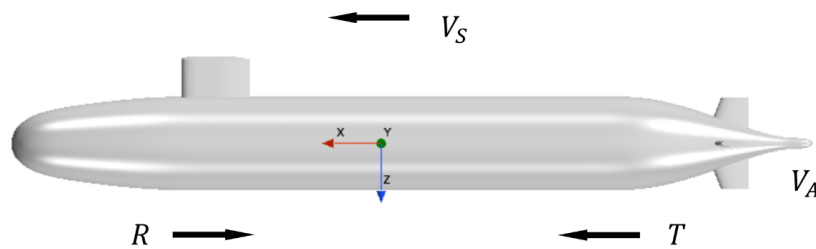(3) The torque Q_B of the propeller is not equal to that of the propeller in the open water for the same thrust.

Figure. 18. Schematic diagram of propeller hull interaction.

The calculated torque Q of the propeller and velocity coefficient J at different propeller rotational speeds are shown in Figure. 19. It can be seen that the propeller torque Q shows an increasing trend as the speed increases, while the velocity coefficient J remains basically unchanged. Moreover, the results forecasted by these two methods are not significantly different. The maximum relative errors of torque and velocity coefficient are 7.37% and -4.41%, respectively. When the propeller rotational speed is close to the self-propulsion point, the torque and velocity coefficient forecasted by the two methods are similar.
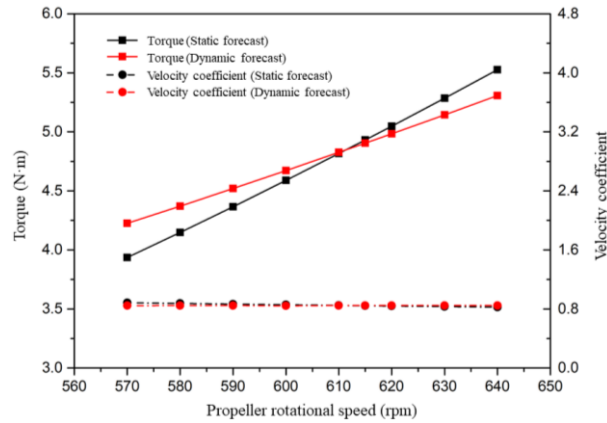
Figure. 19. Variation of torque Q and advance coefficient J with propeller speed.

The thrust and resistance obtained based on these two methods (static forecast and dynamic forecast) are shown in Figure. 20. It can be seen that the thrust and resistance in static forecast are not equal at different propeller rotational speeds except for the self-propulsion point. In dynamic prediction, the thrust and resistance are equal at different propeller rotational speeds. The reason is that the flow field around the hull flows at the speed of 2.75m/s during the static forecast, the propeller is in a light load state when the propeller rotational speed is lower than the self-propulsion point, with the thrust less than resistance and unable to fully utilize the main engine power. Conversely, the hull accelerates from zero speed to a stable speed at a given propeller rotational speed in the process of dynamic forecast. It is in a heavy load state with the thrust greater than resistance, so the calculated thrust and resistance are equal. And when the propeller rotational speed is between 570 and 640 rpm, the range of thrust and resistance changes obtained from the dynamic forecast is smaller than that obtained from the static forecast.
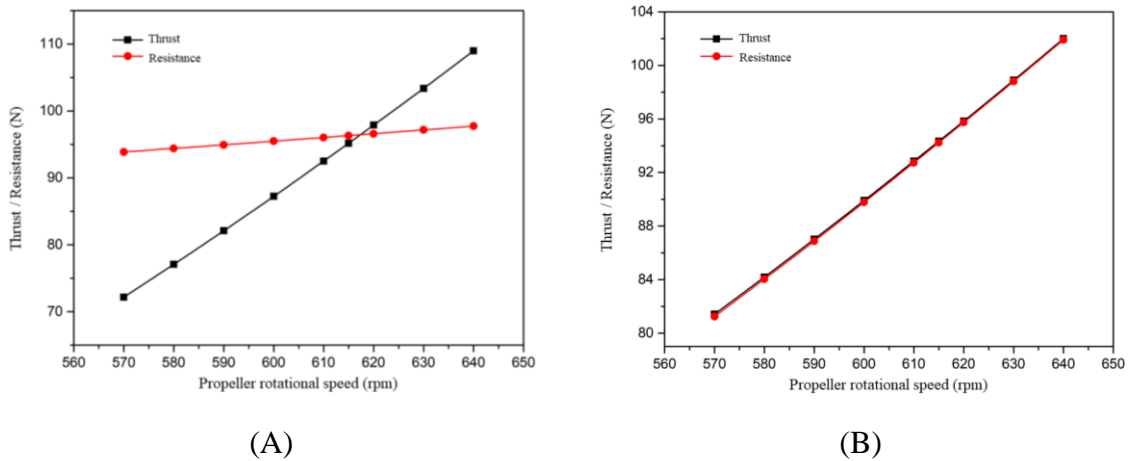

(A)   (B)

Figure. 20. Comparison of thrust and resistance between static forecast and dynamic forecast. (A) Static forecasting results. (B) Dynamic forecasting results.

The thrust coefficient K_T, torque coefficient K_Q, velocity coefficient J, wake fraction ω, thrust deduction coefficient t, and relative rotational efficiency η hydrodynamic performance parameters can be obtained through the self-propulsion calculations. The influence of the underwater vehicle on the propeller is established by the wake fraction ω, because the flow around the hull affects the inlet velocity of the propeller disc. On the contrary, the influence

of the propeller on the underwater vehicle is established by thrust deduction coefficient *t*, because the rotation of the propeller changes the pressure distribution behind the hull, leading to an increase in resistance. The calculation formulas for the relevant parameters are as follows:

$$J = \frac{V_A}{nD} \tag{12}$$

$$K_T = \frac{T}{\rho n^2 D^4} \tag{13}$$

$$K_Q = \frac{Q}{\rho n^2 D^5} \tag{14}$$

$$\eta = \frac{K_{Q0}}{K_{QB}} \tag{15}$$

$$\omega = 1 - \frac{V_A}{V_S} \tag{16}$$

$$t = 1 - \frac{R}{T} \tag{17}$$

Note: The K_{Q0} is the torque coefficient obtained from the open water performance curve of the E1619 propeller using the equal thrust method based on the thrust coefficient behind the hull, K_{QB} is the torque coefficient behind the hull at the self-propulsion point. The resistance *R* in the thrust deduction coefficient is the straight-line navigation resistance when the propeller is not installed behind the underwater vehicle.

The comparison of self-propulsion point parameters between the static forecast and the dynamic forecast is shown in the Table 4. The wake fraction is equal the sum of the frictional wake ω_f, potential wake ω_p and wave-making wake ω_w, and the thrust deduction coefficient *t* is roughly equal to the potential wake ω_p in theory, so in general, the thrust deduction coefficient *t* is smaller than the wake fraction ω, which is verified by the calculations.

Table 4. Comparison of self-propulsion point parameters between static forecast and dynamic forecast.

Method	Rotational speed/rpm	K_T	K_Q	η
Static forecast	617.36	0.193	0.038	98.32%
		ω	t	J
		0.175	0.147	0.842
Dynamic forecast	607.70	K_T	K_Q	η
		0.190	0.038	99.08%
		ω	t	J
		0.183	0.106	0.847

5. Conclusions

In this paper, the self-propelled simulation of the SUBOFF was carried out based on the body force method and the open-water characteristic curve of the E1619 propeller. And the underwater vehicle's self-propulsion point was calculated by using two methods: static forecast and dynamic forecast. The specific conclusions are as follows:

(1) The self-propulsion point obtained from the static and dynamic forecasts at the speed of 2.75 m/s is as follows: the propeller rotational speeds are 617.36 rpm and 607.70 rpm, respectively, and the thrusts are 96.45 N and 92.07 N, respectively. The relative error of the propeller rotational speeds is -1.56%, and that of the thrusts are -4.54%.

(2) By analyzing the hull velocity nephograms obtained by these two forecasting methods, the strip shaped wake generated by the propeller rotation can be seen more clearly. The vortex structures obtained by both static and dynamic forecasting methods are basically the same, and that in the propeller domain is reflected in a circular shape, which cannot capture the tip vortex and blade root vortex well, but can capture the tail wing vortex and the horseshoe vortex at the enclosure.

(3) The calculations of the thrust coefficient, torque coefficient, velocity coefficient, wake fraction, thrust deduction coefficient, and relative rotational efficiency hydrodynamic performance parameters based on the static and dynamic forecasts are close, with the relative errors all within 3%.

References:

1. YANG Qin, WANG Guodong, ZHANG Zhiguo, FENG Dakui, WANG Xianzhou. Numerical Simulation of the Submarine Self-Propulsion Model Based on CFD Technology[J]. Chinese Journal of Ship Research, 2013, 8(2): 22-27. DOI: 10.3969/j.issn.1673-3185.2013.02.005

2. Chase N. Simulations of the DARPA Suboff Submarine Including Self-Propulsion with the E1619 Propeller[D]. The University of Iowa. 2012.

3. Li Peng, Wang Chao, Han Yang, Kuai Yunfei, Wang Shimin. The study about the impact

of the free-surface on the performance of the propeller attached at the stern of a submarine. Chinese Journal of Theoretical and Applied Mechanics, 2021, 53(9): 2501-2514 doi: 10.6052/0459-1879-21-063

4. Çoşgun T. Numerical Self-Propulsion Assessment of a Generic Submarine Model at Various Forward Speeds[J]. Journal of ETA Maritime Science, 2021, 9(3): 192-199.

5. Wang Jianhua. Direct Simulations of Ship Maneuver Using Overset Grid Technique. Ph.D. thesis, Shanghai Jiao Tong Univ., Shanghai, China, 2020.

6. Liao. Hydrodynamic Analysis of Submerged Body During Emergency Surfacing. M.S. dissertation, Harbin Engineering Univ., China, 2018.

7. ZHOU Guangli,DONG Wencai,OU Yongpeng.Numerical simulation of six degree of freedom motion and viscous flow for submarine's emergency ascent[J].Journal of National University of Defense Technology,2017,39(2):199-206

8. MM Amiri, Sp Haier S H, Vitola M A, et al. URANS investigation of the interaction between the free surface and a shallowly submerged underwater vehicle at steady drift[J]. Applied Ocean Research, 2019, 84: 192-205.

9. Sezen S, Delen C, Dogrul A, et al. An investigation of scale effects on the self-propulsion characteristics of a submarine[J]. Applied Ocean Research, 2021, 113.

10. Liu L, Chen M, Yu J, et al. Full-scale simulation of self-propulsion for a free-running submarine[J]. Physics of Fluids, 2021, 33(4): 047103.

11. Kim, Howan, Ranmuthugala, et al. Six-DOF simulations of an underwater vehicle undergoing straight line and steady turning manoeuvres[J]. Ocean Engineering, 2018.

12. Carrica P M, Kim Y, Martin J E. Near-surface self propulsion of a generic submarine in calm water and waves[J]. Ocean Engineering, 2019, 183(JUL.1): 87-105.

13. Carrica P M, Kim Y, Martin J E. Vertical zigzag maneuver of a generic submarine[J]. Ocean Engineering, 2020, 219(4): 108386.

14. Shang H, Zhan C, Liu Z. Numerical Simulation of Ship Maneuvers through Self-Propulsion[J]. Journal of Marine Science and Engineering, 2021, 9(9): 1017.

15. Guo C, Wang X, Wang C, et al. Research on calculation methods of ship model self-propulsion prediction[J]. Ocean Engineering, 2020, 203(6): 107232.

16. Tan. Numerical Study of Hydrodynamic Forces on a Hull with Propeller and Rudder in Maneuvering Motion. M.S. dissertation, Wuhan University of Technology., China, 2019.

17. WANG Huiting, BI Yi. Numerical simulation on planar motion mechanism of KCS ship model with a body-force propeller model[J]. Chinese Journal of Ship Research, 2016, 11(4): 29-37,66. DOI: 10.3969/j.issn.1673-3185.2016.04.005

18. WEI K K, GAO X P. Numerical simulation of emergency surfacing motion of submarine based on volumetric force model[J]. Chinese Journal of Ship Research, 2021, 16(2): 49–56. doi: 10.19693/j.issn.1673-3185.01879

19. Wu. Numerical study of viscous flow around ship hull/propeller/rudder with a body-force propeller. M.S. dissertation, Shanghai, China, 2013.

20. Kim D, Song S, Jeong B, et al. Unsteady RANS CFD simulations of ship maneuverability and course keeping control under various wave height conditions[J]. Applied Ocean Research, 2021, 117: 102940.

21. Wang S, Sun J, Zhao B, et al. Numerical Study on the Interaction between Ocean Current

Power Generator and Unmanned Underwater Vehicle[J]. Journal of Marine Science and Engineering, 2022, 10(12): 1869.

22. Yu J, Yao C, Liu L, et al. Assessment of full-scale KCS free running simulation with body-force models[J]. Ocean Engineering, 2021, 237: 109570.

23. Özden Y A, Özden M C, Demir E, et al. Experimental and numerical investigation of DARPA Suboff submarine propelled with INSEAN E1619 propeller for self-propulsion[J]. Journal of ship research, 2019, 63(04): 235-250.

24. Roddy R F. Investigation of the stability and control characteristics of several configurations of the DARPA SUBOFF model (DTRC Model 5470) from captive-model experiments[J]. David Taylor Research Center, Ship Hydromechanics Department, DTRC/SHD-1298-08, 1990.